Low Temperature Plasma
Technology Laboratory

Nonlocal power deposition in inductively coupled plasmas

John D. Evans and Francis F. Chen

LTP-102 February, 2001

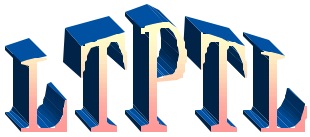

Electrical Engineering Department
Los Angeles, California 90095-1594

Nonlocal power deposition in inductively coupled plasmas

John D. Evans* and Francis F. Chen**

Electrical Engineering Department, University of California, Los Angeles
Los Angeles, California 90095-1594

ABSTRACT

Radiofrequency (rf) plasmas used in the production of computer chips show evidence of field penetration well beyond the classical skin depth. The purpose of this letter is to suggest two physical explanations of this anomaly which could lead to improvements in the design of these important industrial tools. First, by tracing orbits of electrons through many rf cycles in a cylindrical system, it is shown that numerous ionizing electrons can reach the interior. Second, current-carrying electrons can form a long-lived torus which drifts toward the axis, causing the "standing wave" phenomenon observed by previous workers. The pressure dependence of this effect does not agree with collisionless theories of anomalous skin effect but is consistent with the proposed mechanism.

The Anomalous Skin Effect[1] (ASE) has intrigued plasma researchers since the 1960s, when Demirkhanov et al.[2] and others[3] reported non-monotonic decay of rf fields in an overdense plasma. This problem has resurfaced with the use of inductively coupled plasmas (ICPs) in the fabrication of integrated circuits and Micro-Electro-Mechanical Systems (MEMs). Although these rf sources are indispensable for the computer industry, the physics of rf plasma production is not fully understood. In particular, nonlocal phenomena, in which currents do not follow the local value of resistivity, have been observed.[4] We address two such effects: (1) the penetration of rf energy well beyond the classical skin layer, and (2) the non-monotonic behavior of the rf field with radius. Observation of Effect (1) was made in the device shown in Fig. 1, consisting of a 4-turn loop antenna encircling a 30-cm diam, 10-cm long, 1.3-cm thick glass belljar. DC profiles of density $n(r)$, electron temperature $T_e(r)$, and space potential $V_s(r)$ were obtained with an RF-compensated Langmuir probe; and B-dot measurements of the axial RF magnetic field $B_z(r)$ were made with a 5-mm diam, 3-turn magnetic probe in the plane of the antenna. Figure 2 shows that, under typical operating conditions, $n(r)$ is flat or peaked near the axis, even though the RF power is concentrated in a ≈3-cm thick skin layer near the boundary $r = a$, and diffusive losses in the vertical direction should lead to cause a hollow profile. $T_e(r)$ has a small peak in the skin layer, as expected, and both T_e and V_s are nearly constant in the interior region. Similar results were found in a commercial ICP (PlasmaTherm, Inc.), in which even flatter $n(r)$ was obtained via diffusion into the lower chamber. This anomaly has also been reported by Tuszewski[5].

Attempts to explain nonlocal behavior have been based on two concepts: nonlocal conductivity[4,6,7] due to thermal motions (ASE), and the nonlinear ponderomotive force. A kinetic explanation was proposed by Weibel[8] in 1967. In plane geometry, a small class of electrons making a glancing angle with the wall remain in the skin layer long enough to acquire large energies from the E-field induced by the antenna. These fast electrons then wander into the interior of the plasma by virtue of their thermal motions. This theory was extended to cylindrical geometry by Sayasov[9] and has been espoused by many researchers

[4,10-17]. The extensive, ongoing work by Godyak, Piejak, and others[4,11-15] is done with a spiral, stove-top antenna with which the $n(r)$ anomaly was not apparent, since the antenna is radially distributed; indeed, no $n(r)$ profiles were shown. The second proposed mechanism is based on the Lorentz force $\mathbf{F}_L$ due to the RF magnetic field $\mathbf{B}$, which exerts an inward force on the current-carrying electrons and also generates a second-harmonic field at 2ω. The latter effect has been well documented by Piejak, Godyak et al.[18-21] and others[22-25].

By tracing orbits of individual electrons in the RF field, we find that ASE can indeed be explained ~~by~~ as a kinetic effect, but one which is much stronger than predictable from the equilibrium temperature. The curvature of the cylindrical walls causes electrons to impinge upon the wall sheath at steep angles, reflecting them into the center of the discharge. The effect is further enhanced by $\mathbf{F}_L$. This is illustrated in Fig. 3a, showing the path of an electron starting with $|\mathbf{v}| = 0$ at a radius inside the skin layer in an RF field given by $E_\theta = E_0[I_1(k_s r)/ I_1(k_s a)] \sin\omega t$, $B_z = (k_s/\omega) E_0[I_0(k_s r)/ I_1(k_s a)] \cos\omega t$, where I_0, I_1 are Bessel functions, and $k_s \equiv 1/d_s$. In these 2D calculations, the skin depth d_s, the frequency ω, the radius a, and the field strength E_0 are prescribed using experimental values, and the initial particle position (r,θ) and velocity (v_r, v_θ) can be varied, as well as the initial RF phase $\phi_0 = \omega t_0$. When the particle reaches the sheath edge, it is reflected specularly by the Coulomb barrier. We neglect the sheath thickness compared with d_s. Fig. 3a shows that the electron begins to make steep angles with the wall after only a few RF periods and rapidly reaches the interior of the chamber. The Lorentz force $\mathbf{F}_L$ enhances this effect by giving the electron radial momentum. Fig. 3b, together with 3a, shows that the electron energy exceeds the ionization energy only near the wall without $\mathbf{F}_L$ but is large even in the interior with $\mathbf{F}_L$. Individual trajectories depend sensitively on E_0 and the initial values $\mathbf{r}_0$, $\mathbf{v}_0$, and ϕ_0, but examination of many cases reveals several trends: (a) almost all orbits reach the interior after a few RF cycles regardless of $\mathbf{F}_L$, but their energies in the interior are higher when $\mathbf{F}_L$ is included; (b) the effect of $\mathbf{F}_L$ is larger at lower ~~ω's~~ and when the transit time across a diameter is on the order ~~as~~ of an RF period; (c) electrons born in the interior remain in ~~the~~ this weak-field region for many cycles, enhancing $n(r)$ there with their long residence time, but eventually reach the skin layer and get accelerated; (d) the initial thermal velocity of the electrons makes little difference, since they gain much more energy from the RF field.

A more realistic model includes elastic and inelastic collisions, losses of electrons to the wall through the sheath, and the regeneration of electrons through ionization. The electron of motion is

$$d\mathbf{v}/dt = (-e/m)(\mathbf{E} + \mathbf{v}\times\mathbf{B}) - \nu_c \mathbf{v}\,, \qquad (1)$$

where $\mathbf{E}$, $\mathbf{B}$, and collision frequency ν_c are evaluated with the local values of $\mathbf{r}$ and $\mathbf{v}$. The collision probability is recalculated at each time step for a given uniform neutral pressure. If the electron collides elastically, it proceeds with the same velocity in a random direction. Inelastic collisions comprise <0.1% of all collisions and are thus negligible in the orbit calculations. When an electron reaches the sheath or wall, it is reflected specularly unless its perpendicular energy is larger than a prescribed sheath voltage V_{sh}. In the latter case it is lost and replaced by an electron with random $(\mathbf{r}, \mathbf{v})$, weighted according to a prescribed T_e. The values of V_{sh} and T_e are chosen from experimental data. A typical orbit over 67 RF cycles is shown in Fig. 4; discontinuities due to collisions and wall losses can be seen. By following an electron and its reincarnations over many RF cycles, one can construct an ensemble average of the electron energy distribution function (EEDF) and density at each radius. Fig. 5 shows histograms of n and EEDF in four radial sectors of equal area, computed for the

conditions of Fig. 2 and comprising 320,000 (**r**, **v**) pairs. It is seen that there are more low-energy electrons in the weak-field regions, as expected, but that a population of fast electrons capable of ionization exists in all regions, far in excess of those in a Maxwellian distribution. The electron accumulation near the center reduces V_s there, thus increasing $n_i(r)$ locally via reduced ambipolar loss. This mechanism can lead to the centrally peaked density profile of Fig. 2.

Effect (2) is illustrated by Fig. 6, which shows that $|B_z|$ decays radially like a normal evanescent wave until it reaches ≈1% of its maximum amplitude. At $r \sim a/3$, local minima (nodes) appear, as well as a weak maximum on axis. The phase jumps by 180° across each node[26]. Similar profiles have been observed by a number of authors,[2,10,11,13,27] and this effect has been attributed to the collisionless ASE. However, Fig. 6 shows that the "standing wave" effect is more pronounced at higher pressure (collisionality), in contradiction to ASE theory. We propose an alternative physical explanation as follows. Since $\mathbf{F}_L$ preferentially pushes the current-carrying electrons inward, these form a ring of current, which we call a current-carrying structure (CCS), detached from the background electrons. The B-field pattern of the CCS (Fig. 7) resembles a diffuse toroidal theta-pinch. The CCS has an L/R decay time comparable to the RF period. Its current is maintained even for high collisionality because if it should decay faster than the L/R time, the collapsing B-field of the CCS induces an azimuthal E-field that acts to maintain the current. The CCS is formed in the skin layer during a maximum of E ($\phi \sim 0$) and comprises about half of the electron population. Note that the CCS is not composed solely of the fast ionizing electrons found in the orbit calculations above. As the CCS decays in the changing RF field, it is pushed inwards, maintaining an equilibrium position where the magnetic pressures inside and outside the ring are balanced. This motion stagnates at $r/a \approx 1/3$ where the CCS reverses its radial motion. As the RF phase ϕ approaches 90°, the outside pressure drops, and the CCS begins to drift outwards. Near $\phi = 180°$, a new CCS of opposite polarity is formed, and this is pushed inwards until it meets the CCS from the previous half-cycle, which is now much weaker. The new CCS displaces the old (weakened) one, and this process repeats on every half-cycle. Since the CCS decays on its own timescale, it is out of phase with the normal skin current, giving rise to harmonics, which are observed[18].

As a numerical example, assume that the CCS has major radius R and an elliptical cross section with radii b and c, where $c > b$ because of expansion in the unconfined z direction. For definiteness, we consider a current distribution of the bi-Gaussian form

$$j = j_0 \exp[-(r-R)^2/b^2)]\exp(-z^2/c^2)\,. \qquad (2)$$

In its initial position, we assume $R_i = 12$, $b_i = 3$, $c_i = 6$ cm. The self-inductance of this current distribution is computed to be 0.19 μH, and it is approximately doubled to 0.37 μH by the mutual inductance with the background plasma. The resistance, computed for a CCS density of 4×10^{10} cm^{-3}, and a collision rate corresponding to 3-eV electrons in 10 mTorr of Ar, is approximately 3.5 Ω, yielding an L/R time $\tau_{L/R}$ of ≈ 0.1 μsec, comparable to the quarter-cycle time $\tau_{1/4}$ of 0.125 μsec. In its final position, we take $R_f = 5$, $b_f = 2.25$, and $c_f = 4.5$ cm, yielding 0.064 μH and 2.6 Ω, for $\tau_{L/R} = 0.025$ μsec. Thus, the CCS decays more rapidly as it moves inward and e-folds several times during an RF cycle. In Fig. 6, the 20-mTorr data have been fitted with a CCS with $R = 7.5$, $b = 3$, and $c = 6$ cm, imbedded in a classical skin field for $n = 3.1 \times 10^{11}$ cm^{-3}, $p = 20$ mTorr, $KT_e = 3$ eV, and $f = 2$ MHz. Since ν_c/ω is ≈5.4 in this case, this field is significantly different from that in a collisionless, plane plasma[28]. The

current in the CCS was taken to be about four e-foldings below its initial current. There are many adjustable parameters for this fit, but the values are all reasonable.

It is clear that the ratio $\tau_{L/R}/\tau_{1/4}$ determines the magnitude of the "standing wave" effect. If this ratio is too large, the CCS moves back and forth in each cycle, smearing out the null in the time-averaged $|B_z|$. If this ratio is too short, the CCS decays away before reaching a radius where the background field is comparable to its field. Thus, Effect (2) occurs only in an optimal range of pressures and frequencies, as is observed[10].

In conclusion, skin depth anomalies in ICPs can possibly be explained by two new mechanisms proposed here: the reflection of electrons off curved sheaths, and the generation of a detached current ring. The first mechanism suggests that antenna elements near the axis are not necessary for producing uniform plasmas. These effects are, of course, related and have been treated separately only to simplify the discussion. A large numerical simulation would yield an exact EEDF showing both features. Future experiments can be designed to test these ideas, and the required computations may already exist, requiring only further diagnostics.

This work was supported by Applied Materials, Inc., and the Semiconductor Research Corporation with the help of equipment loans from PlasmaTherm, Inc. (now Unaxis) and Hiden Analytical, Ltd. We thank Profs. D. Arnush and G. Tynan for insightful discussions.

FIGURE CAPTIONS

Fig. 1. Schematic of a symmetric, cylindrical ICP test apparatus.

Fig. 2. Profiles of n (10^{11} cm^{-3}), KT_e (eV), V_s (V), and B_z (arbitrary units) in an ICP discharge in 10 mTorr of argon, with P_{rf} = 300W at 2 MHz.

Fig. 3. (a) Path of an electron starting at rest ( ) during the first four cycles of a 6.78 MHz RF field $E_\theta \sin\omega t$, with (marked path) and without (unmarked path) inclusion of the $\mathbf{v} \times \mathbf{B}$ force $\mathbf{F}_L$. The triangles (Δ) mark the positions where E_θ changes sign. The points are 1 nsec apart. The outer circle is the sheath boundary at $r = a$, and the inner circle is smaller by a skin depth of 3.1 cm. $E_\theta(a)$ = - 8 V/cm; B_z (a) = - 7 G. (b) Energy of the electrons following the orbits in (a). The upper curve includes $\mathbf{F}_{NL}$; the lower does not. The line shows the ionization threshold in argon.

Fig. 4. A typical electron trajectory including collisions, losses through the sheath, and replenishment by ionization. Conditions: f = 6.78 MHz, d_s = 3.1 cm, a = 15 cm, E_θ = -8 V/cm, V_{sh} = 20 V, p = 10 mTorr, T_e = 3 eV.

Fig. 5. Monte Carlo calculation of electron energy distribution in four redial regions of equal area. The inset shows the density profile. Conditions: f = 2.0 MHz, d_s = 3.1 cm, a = 15 cm, E_θ = -5 V/cm, V_{sh} = 20 V, p = 10 mTorr, T_e = 3 eV. The curved line is for a 3-eV Maxwellian distribution (log-log scale).

Fig. 6. Normalized semilog plot of $|B_z|$ (r) in the plane of the m = 0 antenna at various pressures. The linear region corresponds to a skin depth of 3 cm. The 5- and 10-mTorr data are connected by lines, but the curve for the 20-mTorr data is a theoretical fit (see text). Conditions: 400W at 2 MHz, 5-20 mTorr of Ar.

Fig. 7. Magnetic field lines around an elliptical, bi-Gaussian CCS with R = 4.5, b = 1.5, and c = 3 cm, imbedded in the time-averaged skin field of an $n = 8 \times 10^{10}$ cm^{-3} plasma with p = 10 mTorr, KT_e = 3 eV, and f = 2 MHz. The box is 15 × 15 cm, and the curvature of the skin field is neglected. For clarity, the CCS current has been given a value higher than what it would be in practice.

REFERENCES

[1] V.I. Kolobov and D.J. Economou, Plasma Sources Sci. Technol. **6**, R1 (1997). This review paper contains extensive references to previous literature.

[2] R.A. Demirkhanov, I.Ya. Kadysh, and Yu. S. Khodyrev, Soviet Phys. JETP **19**, 791 (1964).

[3] M.J. Kofoid and J.M. Dawson, Phys. Rev. Lett. **17**, 1086 (1966).

[4] V.I. Kolobov and V.A. Godyak, IEEE Trans. Plasma Sci. **23**, 503 (1995).

[5] M. Tuszewski, Phys. Rev. Lett. **77**, 1286 (1996).

[6] I.B. Bernstein and T. Holstein, Phys. Rev. **94**, 1475 (1954).

[7] L.D. Tsendin, Sov. Phys. JETP **39**, 805 (1974).

[8] E.S. Weibel, Phys. Fluids **10**, 741 (1967).

[9] Yu. S. Sayasov, Helv. Phys. Acta **52**, 288 (1979).

[10] B. Joye and H. Schneider, Helv. Phys. Acta **51**, 804 (1978).

[11] V.A. Godyak and V.I. Kolobov, Phys. Rev. Lett. **79**, 4589 (1997).

[12] V.A. Godyak and R.B. Piejak, J. Appl. Phys. **82**, 5944 (1997).

[13] R. Piejak, V.A. Godyak, and B. Alexandrovich, J. Appl. Phys. **81**, 3416 (1997).

[14] V.A. Godyak and V.I. Kolobov, Phys. Rev. Lett. **81**, 369 (1998).

[15] V.A. Godyak, R.B. Piejak, B.M. Alexandrovich, and V.I. Kolobov, Phys. Rev. Lett. **80**, 3264 (1998).

[16] S. Takechi, and S. Shinohara, Jpn. J. Appl. Phys. **38**, L148 (1999).

[17] Yu.M. Aliev, I.D. Kaganovich, and H. Schlüter, Phys. Plasmas **4**, 2413 (1997).

[18] V.A. Godyak, R.B. Piejak, and B.M. Alexandrovich, Phys. Rev. Lett. **83**, 1610 (1999).

[19] R.B. Piejak and V.A. Godyak, Appl. Phys. Lett. **76**, 2188 (2000).

[20] A. Smolyakov, V. Godyak, and A. Duffy, Phys. Plasmas **7**, 4755 (2000).

[21] V. Godyak, B. Alexandrovich, R. Piejak, and A. Smolyakov, Plasma Sources Sci. Techn. **9**, 541 (2000).

[22] R.H. Cohen and T.D. Rognlien, Phys. Plasmas **3**, 1839 (1996).

[23] R.H. Cohen and T.D. Rognlien, Plasma Sources Sci. Technol. **5**, 442 (1996).

[24] A.I. Smolyakov and I. Khabibrakhmanov, Phys. Rev. Lett. **81**, 4871 (1998).

[25] C. Chung, S-H. Seo, and H-Y. Chang, Phys. Plasmas **7**, 3584 (2000).

[26] J.D. Evans, F.F. Chen, and D. Arnush, *Investigation of Electromagnetic Field Penetration in ICP and Weakly-Magnetized ICP Discharges*, Proc. Int'l Conf. Plasma Phys., Quebec, Canada (2000), Paper GP1.017

[27] C. Cunge, B. Crowley, D. Vender, and M.M. Turner, *The RF electric field and current density measured in an inductive discharge with a B-dot probe: anomalous skin effect and collisionless power absorption*, Proc. Wksp. on Frontiers in Low Temperature Plasma Diagnostics III (Saillon, Switzerland, 1999), paper N1.

[28] F. F. Chen, *Collisional, magnetic, and nonlinear skin effect in RF plasmas*, UCLA Report LTP-011 (2000), Phys. Plasmas (to be published).

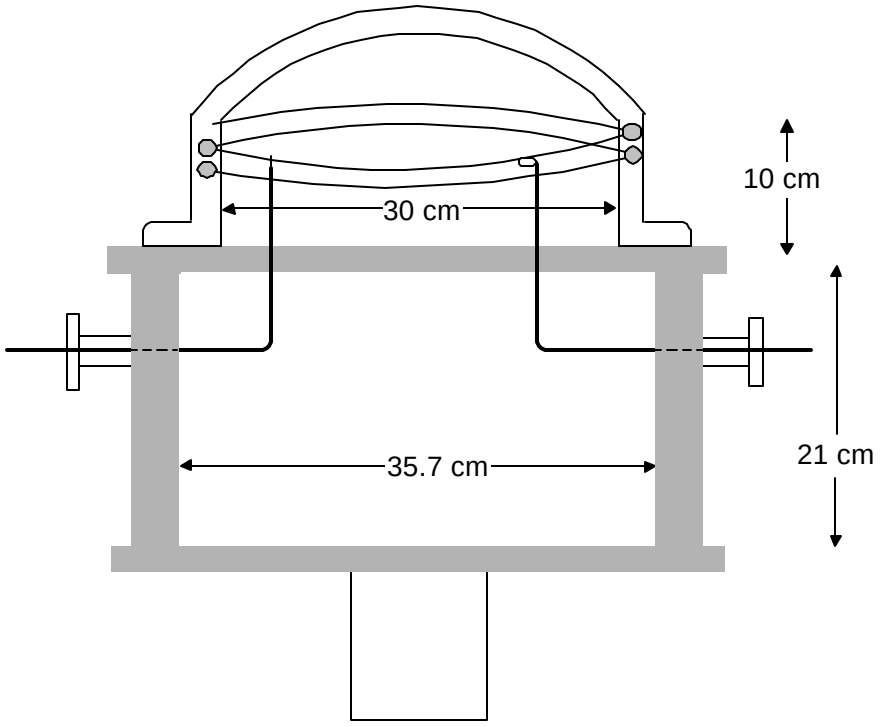

Fig. 1. Schematic of a symmetric, cylindrical ICP test apparatus.

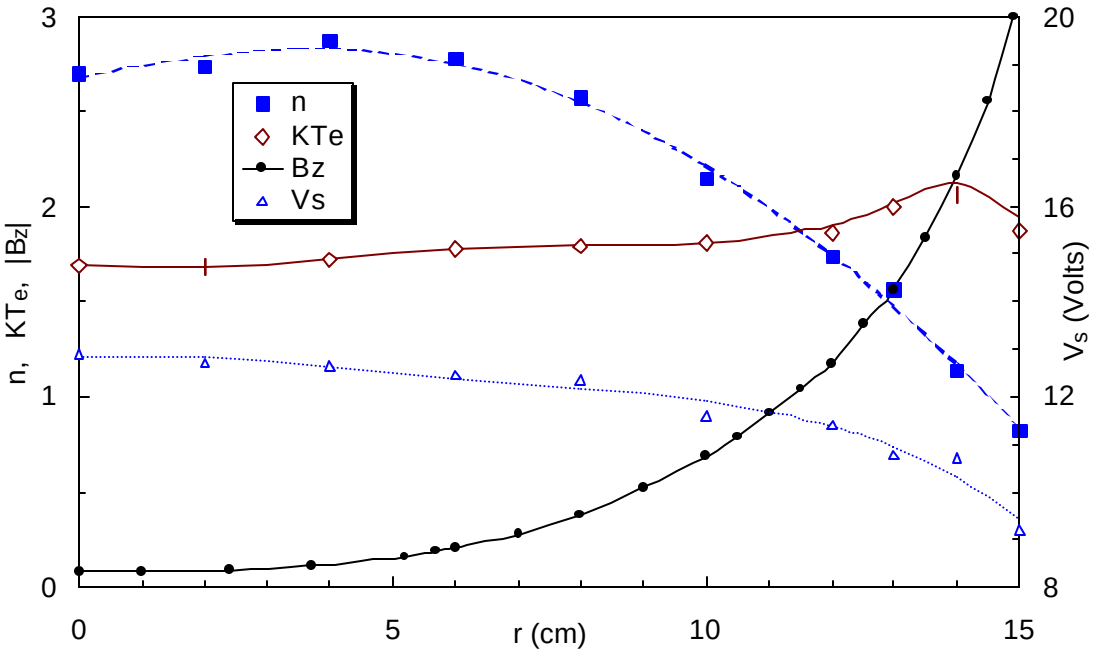

Fig. 2. Profiles of n (10^{11} cm^{-3}), KT_e (eV), V_s (V), and B_z (arbitrary units) in an ICP discharge in 10 mTorr of argon, with P_{rf} = 300W at 2 MHz.

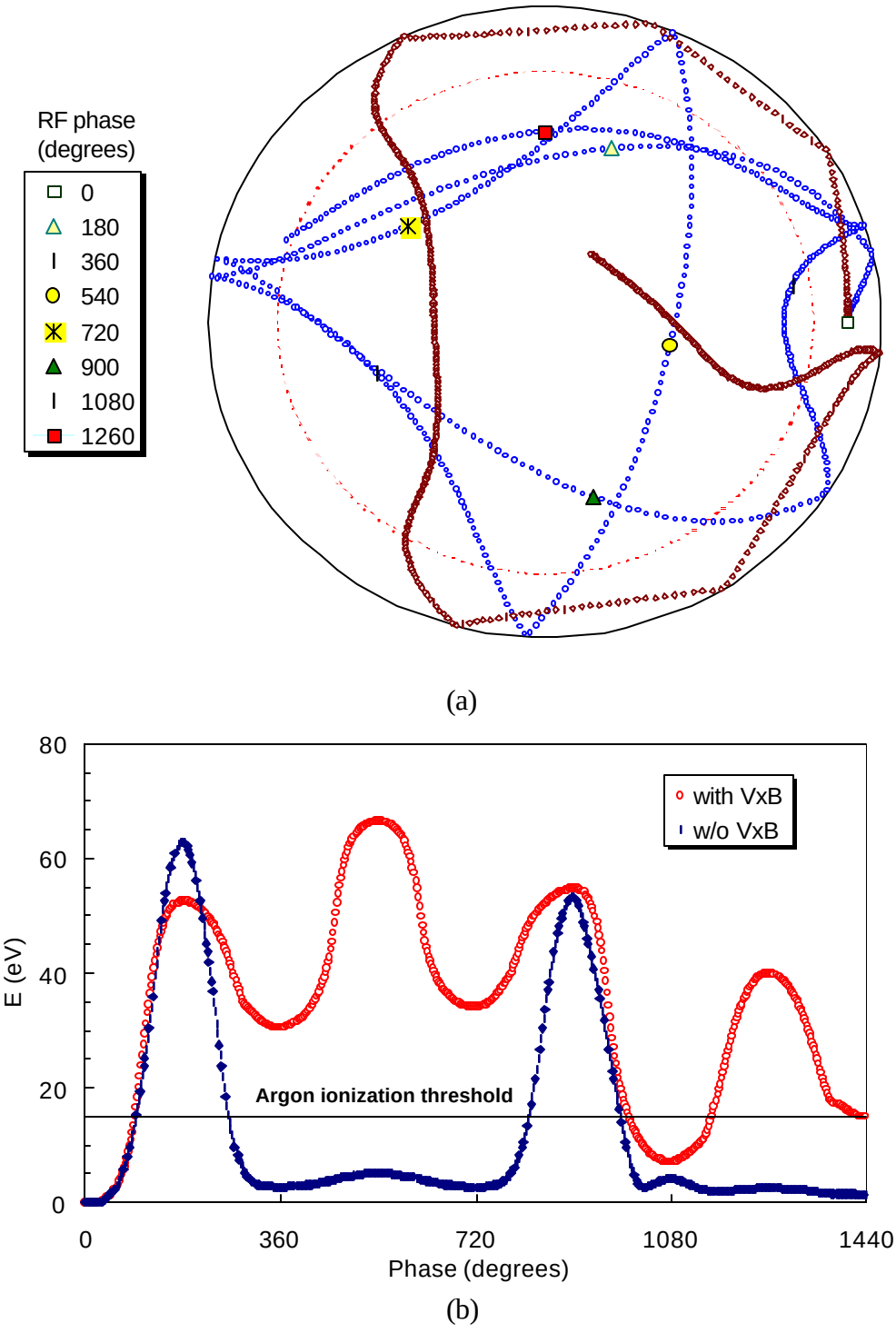

Fig. 3. (a) Path of an electron starting at rest ( ) during the first four cycles of a 6.78 MHz RFfield $E_\theta \sin\omega t$, with (marked path) and without (unmarked path) inclusion of the $\mathbf{v} \times \mathbf{B}$ force $\mathbf{F}_L$. The triangles (Δ) mark the positions where E_θ changes sign. The points are 1 nsec apart. The outer circle is the sheath boundary at $r = a$, and the inner circle is smaller by a skin depth of 3.1 cm. $E_\theta(a)$ = - 8 V/cm; B_z (a) = - 7 G. (b) Energy of the electrons following the orbits in (a). The upper curve includes $\mathbf{F}_{NL}$; the lower does not. The line shows the ionization threshold in argon.

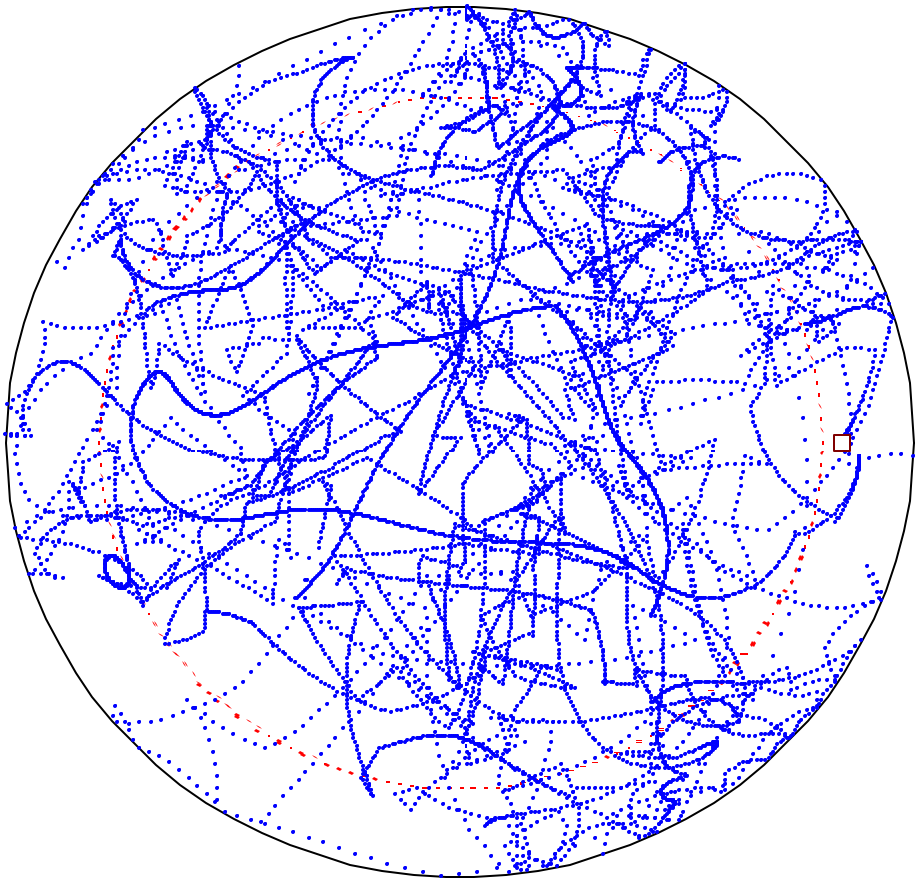

Fig. 4. A typical electron trajectory including collisions, losses through the sheath, and replenishment by ionization. Conditions: f = 6.78 MHz, d_s = 3.1 cm, a = 15 cm, E_θ = -8 V/cm, V_{sh} = 20 V, p = 10 mTorr, T_e = 3 eV.

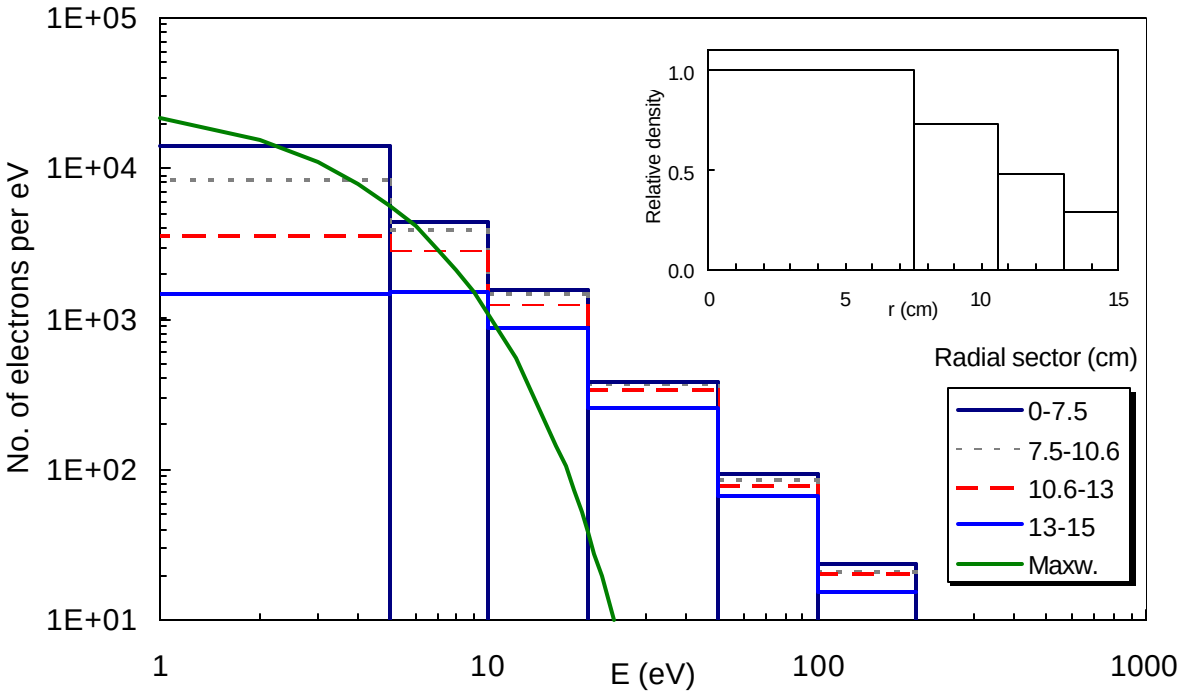

Fig. 5. Monte Carlo calculation of electron energy distribution in four redial regions of equal area. The inset shows the density profile. Conditions: f = 2.0 MHz, d_s = 3.1 cm, a = 15 cm, E_θ = -5 V/cm, V_{sh} = 20 V, p = 10 mTorr, T_e = 3 eV. The curved line is a 3-eV Maxwellian distribution (log-log scale).

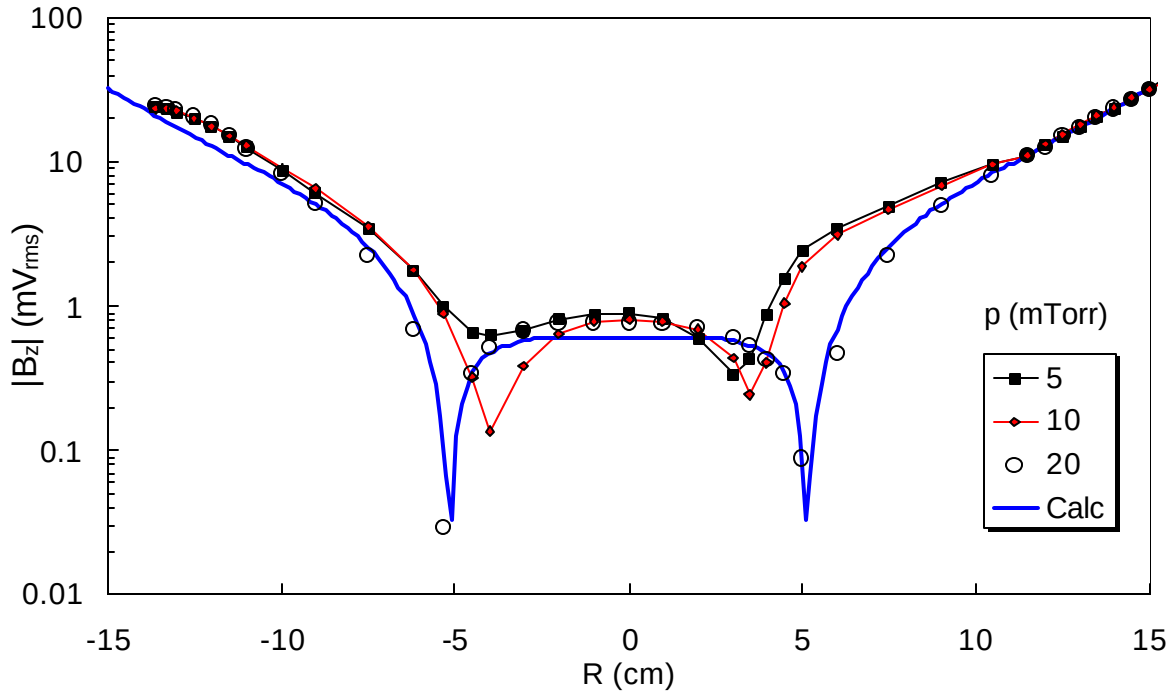

Fig. 6. Normalized semilog plot of $|B_z|$ (r) in the plane of the m = 0 antenna at various pressures. The linear region corresponds to a skin depth of 3 cm. The 5- and 10-mTorr data are connected by lines, but the curve for the 20-mTorr data is a theoretical fit (see text). Conditions: 400W at 2 MHz, 5-20 mTorr of Ar.

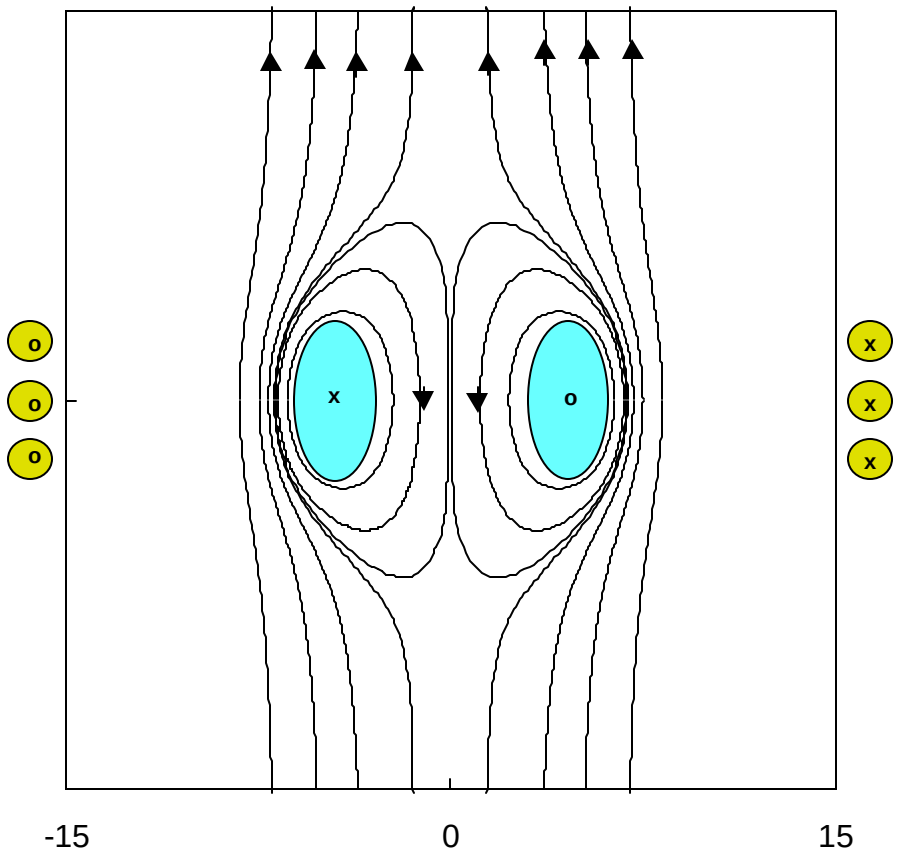

Fig. 7. Magnetic field lines around an elliptical, bi-Gaussian CCS with $R = 4.5$, $b = 1.5$, and $c = 3$ cm, imbedded in the time-averaged skin field of an $n = 8 \times 10^{10}$ cm^{-3} plasma with $p = 10$ mTorr, $KT_e = 3$ eV, and $f = 2$ MHz. The box is 15 × 15 cm, and the curvature of the skin field is neglected. For clarity, the CCS current has been given a value higher than what it would be in practice.